CHAPTER - 4

ANTI CORROSION PROPERTIES OF HYDROXY PYRAZOLINE DERIVATIVES FOR MILD STEEL IN 1M H_2SO_4

4.1 INTRODUCTION

Heterocyclic compounds represent a potential class of corrosion inhibitors. Corrosion inhibition by N containing heterocyclic compounds has been widely reported. The planar π-electrons and lone pair of electrons present on the heteroatoms are the important structural features that determine the adsorption of these molecules on the metal surface. Although a vast number of heterocyclic compounds have been reported as corrosion inhibitors, less work has so far been reported on the use of pyrazolines as corrosion inhibitors for the metals especially mild steel. Pyrazolines are an important class of heterocyclic compounds composed of three carbon atoms and two adjacent nitrogen atoms in a five membered ring system. Among the two nitrogen atoms one is basic and the other is neutral in nature. These are aromatic molecules due to their planar conjugated ring structures with six delocalized π-electrons. The aromatic nature arises from the four π-electrons and the unshared pair of electrons on the –NH nitrogen[1].

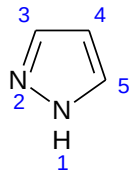

Pyrazolines are considered as a cyclic pyrazine moiety. The C-5 atom is deviated from the almost planar system of the other four atoms of the heterocyclic ring. Pyrazolines are very useful units in the field of medicinal chemistry due to their diverse pharmacological activity and have been reported to exhibit a variety of biological activities.

This chapter is aimed to investigate the role played by newly synthesized hydroxy pyrazoline derivatives on the corrosion inhibition of mild steel in 1M H_2SO_4. The molecular design of the new compounds was based on the fact that, the synthesized hydroxy pyrazolines containing –NH, -OH, >C=O, >C=S and phenyl groups would contribute more effectively towards inhibition of corrosion of mild steel in acid medium. Moreover, they contain reaction centers such as N atoms with lone pair of electrons and aromatic rings with delocalized π-electron systems which can aid their adsorption on the metal surface. To evaluate the inhibition efficiencies of the synthesized compounds in

1M H_2SO_4 solution, electrochemical and non-electrochemical techniques were performed. FTIR was used to identify and confirm the adsorption of the pyrazoline derivatives on the mild steel surface and to provide information about the mechanism of adsorption. The mild steel surface after treatment in the absence and presence of the inhibitors, were analysed by SEM-EDS, XRD and AFM. Theoretical calculations were further employed to explain the inhibition efficiency of the selected synthesized hydroxy pyrazoline derivatives as corrosion inhibitors using density functional theory.

4.2 EXPERIMENTAL WORK

4.2.1 Synthesis of inhibitors

(i) Synthesis of chalcones (I)

Chalcones were prepared by reacting a mixture of acetanilide (0.05 mol), benzaldehyde (0.05 mol), aqueous sodium hydroxide (10%, 5 ml) and methanol (50 ml). The reaction mixture was stirred for 10 hours at room temperature using magnetic stirrer. It was further refluxed for 6 hours on a water bath. After completion of the reaction, the excess solvent was removed by distillation and the resultant viscous mass was poured into ice water (100 ml) with vigorous stirring and left overnight for complete precipitation. The resultant solid was filtered, washed with cold water, dried and recrystallized from ethanol[2].

(ii) Synthesis of dibromochalcone (II)

Chalcone (0.1 mol) in acetic acid (10 ml), bromine (0.125 mol) in acetic acid (10 ml) was added slowly with stirring at 0°C. After complete addition of bromine solution, the reaction mixture was stirred for 5 hours. The solid obtained was filtered and recrystallized from acetone[3].

(iii) Synthesis of acid hydrazides (III $_{a-d}$)

Hydrazine hydrate and methyl benzoate were taken in 1:1 ratio and few ml of alcohol was added to it. This solution was heated in a water bath for half an hour. It was cooled. The precipitated acid hydrazide obtained was filtered, washed and dried. Similar procedure was followed for methyl anthranilate, methyl salicylate and methyl m-nitro benzoate.

(iii) Synthesis of hydroxy pyrazolines (IV $_{a-f}$)

A mixture of dibromo chalcone (4.04 g, 0.01 mol), substituted benzohydrazide (0.012 mol) and triethylamine (3 ml) was heated under reflux in absolute ethanol (15 ml) for 8 hours. The reaction mixture was cooled and poured into ice cold water. The solid separated was filtered, dried and recrystallized from ethanol[3]. (**Scheme: 4.1)**

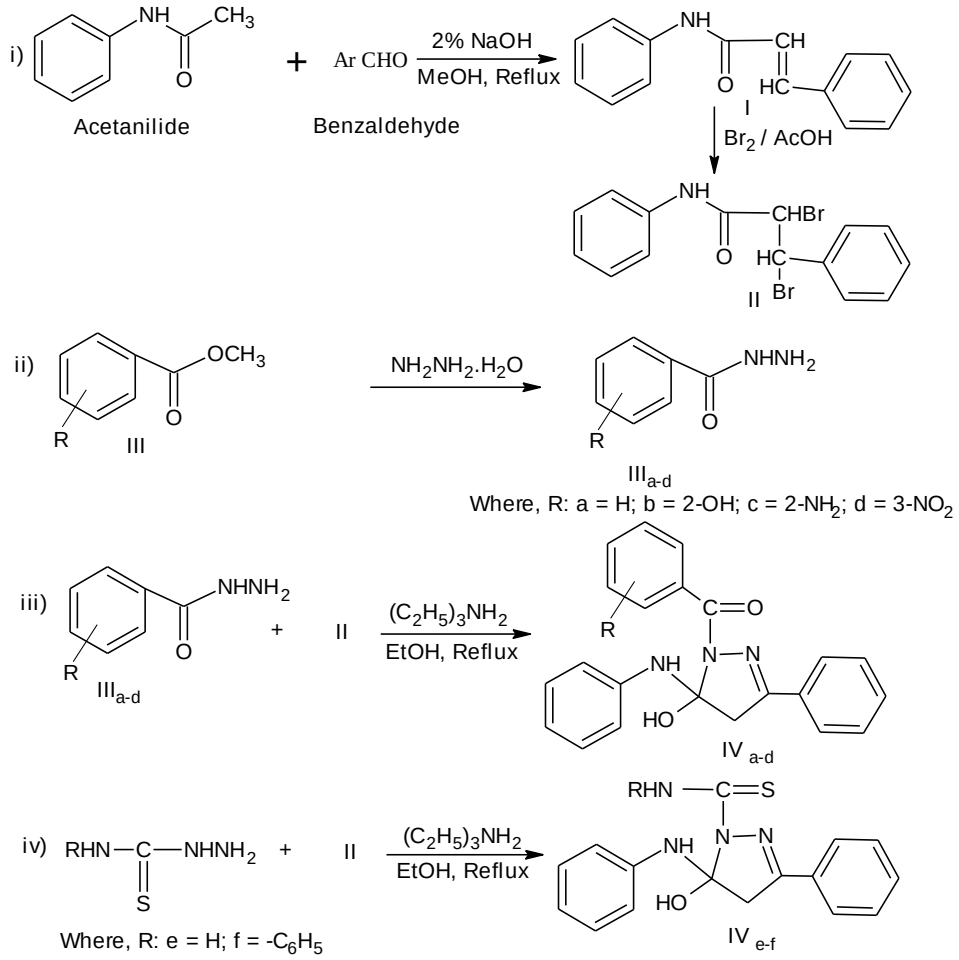

Scheme: 4.1

	R		R		R
IV_a	-H PPM	IV_c	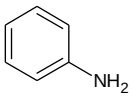 PAPM	IV_e	-H PCT
IV_b	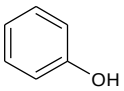 PHPM	IV_d	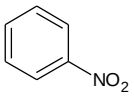 PNPM	IV_f	$-C_6H_5$ PPCT

The synthesized compounds were characterized by FTIR spectra using IR Affinity 1 spectrometer (Shimadzu).

Chemicals used

All chemicals used were of analar grade

Acetanilide, benzaldehyde, aqueous sodium hydroxide, hydrazine hydrate, methyl benzoate, methyl salicylate, methyl anthranilate, methyl m-nitro benzoate, thiosemicarbazide, phenyl thiosemicarbazide, acetic acid, bromine in acetic acid, triethylamine and ethanol.

4.2.2 Evaluation of inhibition efficiency of the hydroxy pyrazolines

4.2.2.1 Non-electrochemical techniques

(i) Weight loss method

The initial weight of the polished specimen was taken. 1M H_2SO_4 was taken in a 100 ml beaker and the specimens were suspended in triplicate into the solution using glass hooks. Care was taken to ensure the complete immersion of the specimen. After a period of three hours, the mild steel specimens were taken out, washed with distilled water, dried and weighed to the accuracy of four decimals. From the initial and final mass of the specimen, (*i.e.,* before and after immersion in the solution) the loss in weight was calculated. The experiment was repeated for various concentrations, (0.5 mM – 10 mM) of the hydroxy pyrazolines (IV_{a-f}).

In order to investigate the effect of temperature on the inhibitor performance, the above procedure was carried out in the different temperature range *i.e.,* 303 - 333 K with one hour immersion time, using a thermostat, with the inhibitor concentration of 10 mM.

(ii) Atomic absorption spectroscopy

Atomic Absorption Spectrophotometer (model GBC 908, Australia) was used for estimating the amount of dissolved iron in the corrodent solution. The polished mild steel specimens were immersed in 1M H_2SO_4 containing various concentration of the hydroxy pyrazolines (0.5 mM - 10 mM). After 3 hours of immersion, the amount of iron in the corrodent solution was determined using AAS. From the amount of dissolved iron, the inhibition efficiency was calculated.

4.2.2.2 Electrochemical techniques

(i) Electrochemical impedance spectroscopy

Electrochemical measurements were performed in a classical three electrode cell assembly with mild steel rod as working electrode (exposed area 0.783 cm^2), a saturated calomel electrode and platinum electrode as reference electrode and counter or auxiliary electrodes. The impedance measurements were carried out IVIUM Compactstat Potentiostat/Galvanostat). The impedance measurements were made at corrosion potentials over a frequency range of 10 kHz to 0.01 Hz with signal amplitude of 10 mV. From the plot of Z′ vs. Z″, the charge transfer resistance (R_{ct}) and double layer capacitance (C_{dl}) were calculated.

(ii) Potentiodynamic polarization method

Polarization measurements were made after EIS studies in the same cell set up for a potential range of -200 mV to +200 mV with respect to open circuit potential at a sweep rate of 1 mV/sec. The log of current and the corresponding potentials were fed out into the plotter and a potential E vs. log I plot was obtained. From the plot, the inhibitor efficiency, Tafel slopes (b_a and b_c) corrosion potential (E_{corr}) and corrosion current (I_{corr}) were calculated using IVIUM software.

4.2.2.3 Surface morphology

Mild steel specimens of size 3 cm × 1 cm × 0.1 cm were immersed in 1M H_2SO_4 in the absence and presence of inhibitors with optimum concentration for 3 hours. The specimens were removed and washed with distilled water and dried at ambient temperature. The chemical composition of the corrosion products were recorded with an EDS detector coupled with SEM using Medzer biomedical research microscope (Mumbai, India), IR spectra using IR Affinity 1 spectrometer (Shimadzu), X-ray diffractometer (XRD; Bruker D8 Advance, Germany) and AFM analysis using Nova 122 software by Multimode scanning probe microscope (NTMDT, NTEGRA prima, Russia).

4.3 RESULTS AND DISCUSSION

4.3.1 Characterization of the synthesized hydroxy pyrazolines

The structural characteristics of the purified pyrazolines (IV_{a-f}) were confirmed by FTIR spectroscopy in the range 4000 – 400 cm^{-1} (Shimadzu, IR Affinity 1). The peaks

around 3180 - 3440 cm^{-1}, 1736 – 1739 cm^{-1} and 1593 - 1634 cm^{-1} are characteristic of –OH/NH, >C=O and >C=N groups respectively. In compounds $IV_{e \text{ and } f}$ the peak at 813.03 cm^{-1} and 819.78 cm^{-1} is characteristic of >C=S stretching absorption band. The structure and physical data of the synthesized inhibitors are presented in Table 4.1. The significant FTIR spectral data of all the hydroxy pyrazolines are tabulated in Table 4.2 and depicted in Figs. 4.1 - 4.6.

4.3.2 Corrosion monitoring techniques

4.3.2.1 Non-electrochemical methods

(i) Gravimetric measurements

Weight loss of mild steel surface in 1M H_2SO_4 was determined at 303 - 333 K in the absence and presence of different concentrations of hydroxy pyrazolines (PPM, PHPM, PAPM, PNPM, PCT and PPCT). The obtained corrosion parameters are presented in Table 4.3 and 4.4. It is clear from the tables that the percentage inhibition efficiency increases with concentration of the inhibitors and decreases with temperature. The compounds exhibited a maximum inhibition efficiency of 80 - 99% at a concentration of 10 mM. The increase in inhibition efficiency with increasing concentrations of the inhibitors at room temperature (303 K) is due to an increase in surface coverage resulting in retardation of the metal dissolution[4]. The efficiency of the inhibitor follows the order

PPCT > PCT > PAPM > PHPM > PPM > PNPM

The data in Table 4.3 reveals that a maximum efficiency of 99.08% and 98.30% was obtained in the presence of 10 mM PPCT and PCT respectively. All the inhibitors have a pyrazole ring, 3 phenyl rings, -NH, >C=O and –OH groups. In addition to these groups, the inhibitors PPCT and PCT have $–NH_2$, >C=S and aryl groups. The maximum inhibition efficiency of the above two compounds is may be due to the presence of the >C=S group[5]. According to **Every** and **Riggs**[6], organic compounds containing nitrogen and sulphur have better inhibition efficiency in acidic media compared to the organic compounds containing nitrogen or sulphur.

(ii) Effect of temperature

The results in Table 4.4 reveal that an increase in temperature decreases the inhibition efficiency. Generally, the metallic corrosion in acidic media is accompanied with evolution of hydrogen gas and rise in temperature usually accelerates the corrosion reactions resulting in higher dissolution rate of the metal[7]. A decrease in inhibition efficiency with temperature can be attributed to the increased desorption of inhibitor molecules from the metal surface or decreased adsorption process suggesting physical adsorption mode. But there are cases where chemical adsorption occurs, although inhibition efficiency decreases with increasing temperature[8].

(iii) Activation parameters of corrosion processes

The activation energy E_a for mild steel in 1M H_2SO_4 in the absence and presence of inhibitors were calculated from the Arrhenius equation and presented in Table 4.5.

$$CR = K \exp\left(\frac{-E_a}{RT}\right) \longrightarrow 4.1$$

where CR is the corrosion rate, R is the molar gas constant, K is the pre-exponential constant, E_a is the activation energy, T is the absolute temperature. Fig. 4.7 represents Arrhenius plot of log CR vs. 1000/T for uninhibited and inhibited solutions. The E_a values were calculated from the slopes of the Arrhenius plots.

From Table 4.5, it is evident that the E_a values are higher in the presence of inhibitors (56.49 - 80.95 kJ mol^{-1}) compared to blank (48.45 kJ mol^{-1}). This is attributed to physical adsorption, where chemical adsorption is more pronounced in the opposite case. The relationship between temperature, percentage inhibition efficiency and E_a in the presence of inhibitors is as follows[9]

(i) For inhibitors, whose percentage inhibition efficiency decreases with increase in T, E_a will be greater than blank.

(ii) For inhibitors, whose percentage inhibition efficiency does not change with temperature, E_a will not change in presence or absence of inhibitors.

(iii) For inhibitors, whose percentage inhibition efficiency increases with increase in temperature, the value of E_a will be less in inhibited solutions compared to uninhibited solutions.

As adsorption decreases more desorption of inhibitor molecules occur because these two opposite processes are in equilibrium. Due to more desorption of inhibitor molecules at higher temperatures, greater surface area of mild steel comes in contact with aggressive environment resulting in an increase in corrosion rates with temperature. The increases in E_a values confirm stronger physisorption of the inhibitors on the mild steel surface. Physisorption is small but important because it is the preceding stage of chemisorption[10].

In order to calculate activation parameters for the corrosion process, Transition state equation was used.

$$CR = \frac{RT}{Nh} \exp\left(\frac{\Delta S^o}{R}\right) \exp\left(-\frac{\Delta H^o}{RT}\right) \longrightarrow 4.2$$

where CR is the corrosion rate, R is the molar gas constant, T is the absolute temperature, h is the Planck's constant, N is Avogadro's number, ΔH^o and ΔS^o are the enthalpy and entropy of activations.

Fig. 4.8 shows a plot of log CR/T as a function of 1000/T for mild steel in 1M H_2SO_4 in the absence and presence of pyrazolines. Straight lines were obtained with slope ($-\Delta H^o/2.303R$) and intercept [$\log(R/Nh) + (\Delta S^o/2.303R)$] from which the values of ΔH^o and ΔS^o were computed and listed in Table 4.5. The values of enthalpy of activation ΔH^o for mild steel at 10 mM of the corrosion inhibitor is higher (53.85 – 78.31 kJ mol^{-1}) than that without the corrosion inhibitor *i.e.,* blank (45.81 kJ mol^{-1}). This may be due to the presence of energy barrier for the reaction, which is the corrosion inhibitor adsorption process that lead to the higher value[11] of ΔH^o. The positive values of enthalpy of activation in the absence and presence of inhibitors indicate an endothermic nature of mild steel dissolution process[12].

The entropy of activation ΔS^o was negative both in the absence and presence of the pyrazolines, implying that the activated complex represented the rate determining step with respect to the association rather than the dissociation step. This implies that a decrease in disorder occurred while proceeding from the reactants to the activated complex. In addition, the less negative value of ΔS^o in the presence of pyrazolines implies that the presence of inhibitor created a near-equilibrium corrosion system state.

(iv) Adsorption isotherm

The organic inhibitors establish their inhibition *via.*, the adsorption of the inhibitor molecules on the metal surface. The adsorption process is influenced by the chemical structures of organic compounds, the distribution of charge in a molecule, the nature and surface charge of metal and the type of aggressive media[13]. Generally, inhibitors may function by physisorption, chemisorption or by complexation with metal ions. Pyrazoline molecules get adsorbed on the mild steel surface due to van der Waals forces. The presence of extensively delocalized π-electrons of the phenyl rings and presence of lone pair of electrons on N, O atoms favour greater adsorption[14]. The adsorption isotherm can provide additional information about the properties of tested compounds. In this study, the surface coverage (θ) is estimated from weight loss measurements to make the fitting and to select the suitable isotherm. The following adsorption isotherms are the most common models to study the mechanism of corrosion inhibition[15]

Temkin adsorption isotherm, $\exp(f \times \theta) = K_{ads} \times C_{inh}$ ⟶ 4.3

Langmuir adsorption isotherm, $\frac{\theta}{1-\theta} = K_{ads} \times C_{inh}$ ⟶ 4.4

Flory–Huggins adsorption isotherm, $\log\left(\frac{\theta}{C_{inh}}\right) = \log(K_{ads}) + a \times \log(1-\theta)$ ⟶ 4.5

where K_{ads} is the equilibrium constant of the adsorption process, C_{inh} is the inhibitor concentration, f is the factor of energetic inhomogeneity and the parameter 'a' in Eq. 4.5 is the number of water molecules replaced by inhibitor molecules on metal surface.

For each inhibitor, Temkin, Flory–Huggin and Langmuir isotherm were fitted which are shown in the (Figs. 4.9 - 4.11). Table 4.6 and 4.7 show the corresponding fitting curve results where R^2 is the square of the correlation coefficient between the dependent variables and the estimated values by the regressors, or equivalently defined as the ratio of regression variance to total variance. It is seen that the best fit is obtained for the Langmuir isotherm model. The phenomenon of interaction between the metal surface and the inhibitor can be better understood in terms of the adsorption isotherm. In addition, Fig. 4.11 shows the relationship between C/θ and C (Langmuir isotherm) for the pyrazolines, which yields a straight line with an approximately unit slope, indicating that the inhibitor under study obeys the Langmuir adsorption isotherm[16]. This isotherm

assumes that the adsorbed molecules occupy only one site and there are no interactions with other adsorbed species. According to this isotherm, θ is related to the inhibitor concentration C and adsorption equilibrium constant K_{ads} *via.*,

$$\frac{C}{\theta} = \frac{1}{K_{ads}} + C \qquad \longrightarrow \quad 4.6$$

The value of equilibrium constant can be calculated from the intercept of Langmuir plots. The high value of the adsorption equilibrium constant K_{ads} reflects the high adsorption ability of the inhibitors on the mild steel surface. Further, this constant is related to the standard Gibb's free energy of adsorption (ΔG^{0}_{ads}) by the following equation

$$\Delta G^{\circ}_{ads} = -RT \ln(55.5\ K_{ads}) \qquad \longrightarrow \quad 4.7$$

where 55.5 represents the molar concentration of water in solution (mol L^{-1}), R is the molar gas constant and T is the absolute temperature. Table 4.7 represents the results derived from the application of Langmuir's relationship, for the pyrazolines. From the results obtained, it is significant to note that the R^2 values and the slope values of the plots are very close to unity, which indicates a strong adherence of the adsorption data to the assumptions establishing Langmuir adsorption isotherm. The negative values of ΔG^{o}_{ads} suggest that the adsorption of pyrazolines on the mild steel surface is spontaneous. Generally, values of ΔG^{o}_{ads} around -20 kJ mol^{-1} or lower are consistent with the electrostatic interaction between the charged molecules and the charged metal (physisorption); those around -40 kJ mol^{-1} or higher involves sharing or transfer from organic molecules to the metal surface to form a co-ordinate type of bond (chemisorption), while values between -20 kJ mol^{-1} and -40 kJ mol^{-1} indicate both physisorption and chemisorption[16]. In the present case ΔG^{o}_{ads} values are around -30 kJ mol^{-1}, which means that the adsoprtion of pyrazolines on the mild steel surface invloves both physisorption and chemisorption.

(iv) Thermodynamic parameters

The thermodynamic functions such as the free energy of adsorption (ΔG^{o}_{ads}), the enthalpy of adsorption (ΔH^{o}_{ads}) and the entropy of adsorption (ΔS^{o}_{ads}) are very important to explain the adsorption phenomenon of inhibitor molecule. Thermodynamically, ΔG^{o}_{ads} is related to the standard enthalpy and entropy of adsorption process, ΔH^{o}_{ads} and ΔS^{o}_{ads}

respectively *via.,* Equation 4.8 and the standard enthalpy of adsorption ΔH^{o}_{ads} can be calculated according to the Van't Hoff equation[17]

$$\Delta G^{o}_{ads} = \Delta H^{o}_{ads} - T\Delta S^{o}_{ads} \longrightarrow 4.8$$

$$\ln K_{ads} = -\frac{\Delta H^{o}_{ads}}{RT} + \frac{\Delta S^{o}_{ads}}{T} + \ln\frac{1}{55.5} \longrightarrow 4.9$$

A plot of ln K_{ads} vs. 1000/T gives a straight line, as shown in Fig. 4.12. The slope of the straight line is (ΔH^{o}_{ads}/R). The value of ΔH^{o}_{ads} is given in Table 4.8. Since the ΔH^{o}_{ads} value is negative, the adsorption of inhibitor molecules on the mild steel surface is an exothermic process, chemisorption is distinguished from physisorption by considering the absolute value of ΔH^{o}_{ads} . ΔH^{o}_{ads} values lower than -40 kJ mol^{-1} indicate physical adsorption and values approaching -100 kJ mol^{-1} indicate chemical adsorption[18]. In the present case, ΔH^{o}_{ads} values are below -40 kJ mol^{-1} confirming the possibility for physisorption.

The value of ΔH^{o}_{ads} found by the Van't Hoff equation, may also be evaluated by the Gibb's Helmholtz equation, which is defined as follows

$$\frac{\partial(\Delta G^{o}_{ads}/T)}{\partial T} = \frac{-\Delta H^{o}_{ads}}{T^{2}} \longrightarrow 4.10$$

This equation can be arranged to give

$$\frac{\Delta G^{o}_{ads}}{T} = \frac{\Delta H^{o}_{ads}}{T} + K \longrightarrow 4.11$$

The variation of ΔG^{o}_{ads}/T with 1/T (Fig. 4.13) gives a straight line with slope equal to ΔH^{o}_{ads}. It can be seen from the figure that ΔG^{o}_{ads}/T decreases with 1/T in a linear fashion. The calculated values are shown in Table 4.8 confirming the exothermic behaviour of adsorption on the steel surface, therefore the values of ΔH^{o}_{ads} obtained by both methods are in good agreement.

The free energy of adsorption (ΔG^{o}_{ads}) calculated for pyrazolines were between 25.42 - 33.46 kJ mol^{-1}. This value confirmed the mixed mode of adsorption of the pyrazolines on the mild steel surface.

4.3.2.2 Atomic absorption spectrophotometric studies

The amount of iron dissolved in the absence and presence of pyrazolines were calculated for the mild steel specimens immersed in 1M H_2SO_4 containing 0.5 mM and

10 mM concentrations and are presented in Table 4.9**.** It has been found that the amount of dissolved iron in the corrodent solution decreases with increase in concentration of the inhibitors and there is good agreement between values of percentage inhibition efficiency calculated from weight loss and AAS techniques.

4.3.3 Electrochemical mesasurements

4.3.3.1 Electrochemical impedance spectroscopy (EIS) measurements

The results of the potentiodynamic polarization experiments were confirmed by impedance measurements, since the electrochemical impedance spectroscopy (EIS), is a powerful technique in studying corrosion mechanisms and adsorption phenomena. EIS measurements were carried out for corrosion of mild steel in 1M H_2SO_4 in the absence and presence of pyrazolines (PPM - PPCT) at 303 K. The Nyquists plot for mild steel in the absence and presence of pyrazolines (PPM - PPCT) are presented in Figs. 4.14 a-f. It has been reported by **Jones**[19], that the semicircles at high frequencies are generally associated with the relaxation of electrical double-layer capacitors and the diameters of the high-frequency capacitive loops can be considered as the charge-transfer resistance. The diagram of the capacitive loop obtained increases in the presence of inhibitor and was indicative of the degree of inhibition of the corrosion process. The high frequency limits corresponding to the solution resistance R_s (Ω), while the lower frequency limits corresponds to (R_{ct} + R_s). The low frequency contribution showed the kinetic response of the charge transfer reaction[20]. The impedance parameter such as charge transfer resistance (R_{ct}), double layer capacitance (C_{dl}) and inhibition efficiency (% IE) were calculated and are listed in Table 4.10. The charge transfer resistance (R_{ct}) values were calculated from the difference in real impedance (Z_r) at lower and higher frequencies[21]. The double layer capacitance can be determined from the relationship

$$C_{dl} = \frac{1}{2\pi R_{ct} f(-Z_i max)} \longrightarrow 4.12$$

where $f(-Z_i\,max)$ is the frequency at which the imaginary part of the impedance is maximum. R_{ct} and C_{dl} derived from the impedance measurements are shown as a function of inhibitor concentration. The R_{ct} values increase and the C_{dl} values decrease with increasing concentration of the inhibitors and hence, the inhibition efficiency (% IE) increases. The charge transfer resistance, which controls the overall corrosion process,

showed an increase with increasing inhibitor concentration. However, the capacity of the double layer decreased as inhibitor concentration increased. The double layer between charged metal surface and solution is considered as electrical capacitor and it is generally assumed that acid corrosion inhibitors adsorb on metal surface resulting in a structural change of double layer and reduced rate of electrochemical partial reaction. In the system under investigation, the decrease in electrical capacity of the working electrodes surface in the presence of the different inhibitors could be correlated with the decrease in the corrosive area on the electrode surface owing to the increase of the area covered with the adsorbed inhibitor molecules[21].

4.3.3.2 Potentiodynamic polarization measurements

Polarization measurements are suitable for monitoring the progress and mechanisms of the anodic and cathodic partial reactions[22]. Potentiodynamic polarization experiments were undertaken to determine the effect of the anodic ($Fe \longrightarrow Fe^{2+} + 2e^-$) and cathodic ($2H^+ + 2e^- \longrightarrow H_2$) partial reactions of the corrosion process. Typical potentiodynamic polarization curves for the mild steel specimens in 1M H_2SO_4 without and with different concentrations of hydroxy pyrazolines (PPM – PPCT) are shown in Figs. 4.15 a-f. The polarization curves reveal that the mild steel specimen exhibit active dissolution with no distinctive transition to passivation within the studied potential range in the acidic environment. The plots also show that the anodic and cathodic reactions in blank acid and upon addition of the pyrazolines follow Tafel's law. The linear Tafel segments of the anodic and cathodic curves were extrapolated to corrosion potential to obtain the corrosion current densities (I_{corr}). The corresponding electrochemical parameters namely corrosion current densities (I_{corr}), corrosion potential (E_{corr}), the cathodic Tafel slope (b_c) and the anodic Tafel slope (b_a) derived from the polarization curves are presented in Table 4.11. Results in Table 4.11 indicate that the corrosion current density decreased markedly in the presence of inhibitors compared to the blank solution. The decrease is due to the blocking of the mild steel surface by adsorption of the inhibitor molecules through active centres. This is evident from the shift of E_{corr} in the negative direction with respect to blank signifying the suppression of the cathodic reaction. The addition of the inhibitors to the aggressive medium have changed the values of both b_a and b_c but b_c to a greater extent. This indicates that the inhibitors have affected

the anodic dissolution of iron as well as cathodic evolution of hydrogen. The mixed nature of the inhibitors can be explained in terms of a change in E_{corr} values in the presence of inhibitors. If the displacement in E_{corr} values in the presence of inhibitors is more than $\pm$85 mV/SCE related to E_{corr} of blank, the inhibitor can be considered as anodic or cathodic[22, 23]. If the change in E_{corr} is less than $\pm$85 mV/SCE, the corrosion inhibitor may be regarded as a mixed type. The maximum displacement in our study is 78.5 mV/SCE which indicates that the pyrazolines act as mixed type inhibitors. However, in (Figs. 4.15 a-f) the minor shift of E_{corr} values towards negative direction suggests the predominant cathodic control over the reaction.

4.3.4 Surface characterization

4.3.4.1 FTIR analysis of mild steel plate

Figs. 4.16 - 4.17 shows the FTIR spectra of mild steel plates immersed in 10 mM of PPM and PPCT for 3 hours. In the IR spectra of PCT and PPCT bands characteristics of -NH, -OH, >C=O, >C=S and >C=N- observed around 3200 cm^{-1}, 3300 cm^{-1}, 1700 cm^{-1}, 800 cm^{-1}, 1600 cm^{-1} were also present in the FTIR spectra of the mild steel plate immersed in 1M H_2SO_4 containing 10 mM PCT and PPCT, confirming the presence of the inhibitors on the metal surface. Thus, the FTIR spectra of mild steel plates further substantiate the fact that the hydroxy pyrazolines are good corrosion inhibitors for mild steel in H_2SO_4 medium.

4.3.4.2 Scanning electron microscope-Energy dispersive X-Ray spectroscopy (SEM-EDS)

In order to evaluate the conditions of the mild steel surfaces in contact with acid solution, a superficial analysis was carried out. The SEM micrographs of mild steel specimen in 1M H_2SO_4 solution in the absence and presence of inhibitors (PAPM and PPCT) after 3 hour exposure are given in Figs. 4.18 - 4.20. In Fig. 4.18, the mild steel surface is strongly damaged in the absence of inhibitors due to metal dissolution in corrosive solution. However the appearance of steel surface was significantly different after the addition of inhibitors (PAPM and PPCT) to the corrosive solution. It can be seen from Figs. 4.19 - 4.20 that, the dissolution rate of mild steel considerably reduced and the smooth surface appeared by formation of a good protective film upon adsorption of

inhibitor molecules on the metal surface, which was responsible for the inhibition of corrosion.

The EDS spectra were used to determine the elements present on the surface of mild steel in the uninhibited and inhibited 1M H_2SO_4. The EDS analysis of uninhibited mild steel plate indicate the presence of only Fe and oxygen confirming that passive film on the mild steel surface contained only Fe_2O_3 (Fig. 4.21). Figs. 4.22 - 4.23 portray the EDS analysis of mild steel in 1M H_2SO_4 in the presence of pyrazolines (PAPM and PPCT). EDS spectrum of PAPM (Fig. 4.22) shows the additional lines due to C, O and N in comparison to EDS spectrum (Fig. 4.21) of blank. However in the presence of the optimum concentration of the inhibitors, appearance of nitrogen and carbon bands were observed due to the formation of a strong protective film of the inhibitor molecules on the mild steel surface. This clearly indicates that the nitrogen atom present in the inhibitor molecules is involved in the adsorption process with metal atom and hence protects the metal surface against corrosion. This spectrum confirms the presence of the pyrazoline molecules on mild steel surface[24].

EDS spectrum of PPCT **(**Fig. 4.23) shows additional lines characteristic of N and S. In addition, the intensites of C and O signals are enhanced. The appearance of the N and S signal and this enhancement in the C and O signals confirms the presence of pyrazoline molecules on the metal surface. From the two EDS spectra, it is evident that the Fe peaks are considerably suppressed in the presence of inhibitors (PAPM and PPCT) which may be attributed due to the overlying inhibitor film[25]. A comparable elemental distribution obtained from the spectra was presented in Table 4.12.

4.3.4.3 X-ray diffraction patterns

The chemical characterization of the oxide layer formed on metals and the understanding of its formation mechanisms are important factors for the development and improvement of materials for corrosion resistance. The corrosion products formed on mild steel exposed to acid medium have been studied by X-ray diffraction method. The main phases reported are lepidocrocite (g-FeOOH), goethite (a-FeOOH) and magnetite (Fe_3O_4). Lepidocrocite is usually formed in the early stages of atmospheric corrosion but as the exposure time increases it is transformed into goethite[26]. The patterns obtained clearly reveal the presence of metal and metal oxide phases. In Fig. 4.24 (blank), the

peaks at 2θ = 28.2, 35.3, 44.2 and 64.1° can be assigned to oxides of iron. Thus, the surface of the metal immersed in 1M H_2SO_4 contains iron oxides, which are most probably lepidocrocite (g-FeOOH) and magnetite (Fe_3O_4). The XRD pattern for the metal immersed in the 1M H_2SO_4 containing optimum concentration of PPCT is given in Fig. 4.25. The intensity of the peaks due to oxides of iron, such as goethite (a-FeOOH) and magnetite (Fe_3O_4) are found to be very low and the peaks due to iron alone observed at 2θ = 44.4, 65 and 82.6° are very high. This confirms the protection of the mild steel by hyroxy pyrazolines.

4.3.4.4 Atomic force microscopy

AFM is a powerful technique to investigate the surface morphology at nano to micro scale and has become a new choice to study the influence of inhibitor on the generation and the progress of the corrosion at the metal-solution interface. The two dimensional (2D) and three dimensional (3D) AFM studies for mild steel surface immersed in 1M H_2SO_4 (blank) and mild steel surface immersed in 1M H_2SO_4 containing inhibitor have been carried out and the 2D and 3D morphological images are presented in Figs. 4.26 - 4.27. AFM imaging studies were carried out to obtain the average roughness (R_a), root-mean-square roughness (R_q) and the maximum peak to valley (P−V) height values[27, 28]. From the data, it is obvious that the steel surface was protected in the presence of the inhibitor. Hence, the average R_a (126.19 nm for blank and 82.60 nm for PPCT), Rq (175.77 nm for blank and 104.30 nm for PPCT) and P−V height values (1447.55 nm for blank and 781.87 nm for PPCT) were less compared to the uninhibited solution. The decrease in the average R_a, R_q and P-V height values, confirmed the formation of the protective layer of PPCT molecules on the mild steel surface.

4.3.5 Quantum chemical studies

4.3.5.1 Quantum chemical study of non-protonated form of the studied inhibitors in aqueous phase

In order to study the effect of molecular structure on the inhibition efficiency, quantum chemical calculations were performed on the selected hydroxy pyrazoline derivatives namely PPM, PHPM and PCT in non-protonated and protonated forms. The computed quantum chemical properties such as energy of highest occupied molecular

orbital (E_{HOMO}), energy of lowest unoccupied molecular orbital (E_{LUMO}), the energy band gap (ΔE), hardness, softness, number of electrons transferred (ΔN) and dipole moment (μ) in non-protonated and protonated forms are summarized in Table 4.13 and 4.16. Most of the quantum chemical parameters in non-protonated form do not correlate with the predicted experimental inhibition efficiencies of hydroxy pyrazolines.

4.3.5.2 Quantum chemical study of protonated form of the studied inhibitors in aqueous phase

The presence of heteroatoms in the molecules of hydroxy pyrazoline derivatives suggests high tendency towards protonation in acidic solution. Therefore it is important to investigate the protonated forms of the studied structures in order to determine the preferred form of the hydroxy pyrazolines to interact with the metal surface in acid solution. The results also show that preferred site for adsorption of hydroxy pyrazolines are PPM (N15, N29), PHPM (N14, N28) and PCT (N3, N17) atoms because it is the least sterically hindered heteroatom and has adequate negative partial charge.

It is well documented in literature that the higher the HOMO energy of the inhibitor, higher is the corrosion inhibition efficiency. It is evident from Table 4.16 that PCT has the highest E_{HOMO} in the protonated form. This means that the electron donating ability of PCT is stronger in the protonated form. This confirms the experimental results that interaction between PCT and mild steel is electrostatic in nature (physisorption). The adsorption of inhibitor (PCT) on a metallic surface occurs at the part of the molecule which has the greatest softness (0.9765) and lowest hardness. It is evident from Table 4.16 that, E_{HOMO}, softness and fraction of electrons transferred followed the order PCT > PHPM > PPM which is consistent with the obtained experimental order.

In addition, the lower the LUMO energy, the easier the acceptance of electrons from the metal surface, and as the LUMO – HOMO energy gap decreased, the efficiency of inhibitor (PCT) has improved. Quantum chemical parameters such as E_{LUMO}, energy gap, hardness are listed in Table 4.16 indicate that PCT is an efficient inhibitor in H_2SO_4 and followed the order PCT < PHPM < PPM which corresponds to the experimental results.

4.3.5.3 Mulliken charge density distribution

Mulliken charges for non-protonated species (Table 4.14) reveal that the inhibitors had a considerable excess of negative charge around the nitrogen and oxygen atoms present in pyrazoline ring and in some, carbon atoms and sulphur atoms, indicating that these are the adsorption sites of the inhibitors. The Mulliken atomic charges on the atoms of the protonated species of pyrazoline derivatives are reported in Table 4.17 and are compared with the corresponding Mulliken atomic charges of the non-protonated species. In protonated forms of the studied inhibitors, some C, N and S atom possess high negative charge and are responsible for the strong adsorption of the inhibitors on the metal surface. Table 4.15 and 4.18 shows the optimized structure, HOMO and LUMO orbital contributions for the non-protonated and protonated forms of the selected hydroxy pyrazolines.

4.3.6 Mechanism of corrosion inhibition

The adsorption of pyrazoline derivatives can be attributed to the presence of polar unit having atoms of nitrogen, oxygen, sulphur and aromatic/heterocyclic rings. Therefore the possible reaction centers are unshared electron pairs of heteroatoms and π-electrons of aromatic ring[29].

Corrosion inhibition of mild steel in 1M H_2SO_4 by pyrazolines can be explained on the basis of molecular adsorption on the metal-solution interface. In aqueous acidic solutions, pyrazoline derivatives exist either as neutral molecules or as protonated molecules and may adsorb on the metal-acid solution interface by one and/or more of the following ways:

(i) Electrostatic interaction of protonated molecules with already adsorbed sulphate ions.

(ii) Donor-acceptor interactions between the π-electrons of aromatic rings and vacant d-orbital of surface iron atoms.

(iii) Interaction between unshared electron pairs of hetero-atoms and vacant d-orbital of iron surface atoms.

In general, two modes of adsorption are considered on the metal surface in acid medium. In the first mode, neutral molecules may be adsorbed on the surface of mild steel through the chemisorption mechanism, involving the displacement of water molecules from the mild steel surface and the sharing electrons between the hetero-atoms

and iron. The inhibitor molecules can also adsorb on the mild steel surface on the basis of donor-acceptor interactions between π-electrons of the aromatic ring and vacant d-orbitals of surface iron atoms.

In the second mode, since it is well known that the steel surface bears positive charge in acid solution[30], it is difficult for the protonated molecules to approach the positively charged steel surface due to the electrostatic repulsion. But sulphate ions have a smaller degree of hydration and these ions could bring excess negative charges in the vicinity of the interface and favour more adsorption of the positively charged inhibitor molecules.The protonated pyrazolinium ion adsorb through electrostatic interactions between the positively charged molecules and the negatively charged metal surface. Thus, we can conclude that inhibition of mild steel corrosion in 1M H_2SO_4 is mainly due to electrostatic interaction. The decrease in inhibition efficiency with rise in temperature supports electrostatic interaction[31, 32].

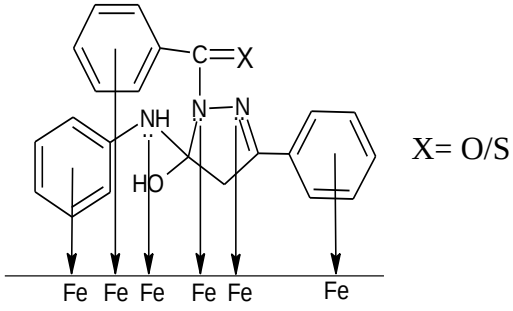

Fig. i

Fig. i: Represents schematic diagram of adsorption of hydroxy pyrazolines on mild steel surface

4.3.7 Evaluation of pyrazolines: Chemical structure of the inhibitors and its effect on the corrosion inhibition

Inhibition efficiency of the investigated compounds depends on many factors which include the number of adsorption active centers in the molecule, their charge density, molecular size and mode of interaction with metal surface. It is generally believed that the adsorption of the inhibitor at the metal-solution interface is the first step in the mechanism of inhibitor action in aggressive acid media. The order of inhibition efficiency of the tested pyrazolines follows the order:

PPCT > PCT > PAPM > PHPM > PPM > PNPM

All the synthesized pyrazolines exhibit a maximum inhibition efficiency of 80 to 99% at a concentration of 10 mM. The highest inhibition efficiency of these compounds is due to the presence of π-electrons on the pyrazole and benzene rings, -NH, C=N, C=O, OH groups and electron releasing substituents in the aromatic rings such as OH, NH_2 which enhances the electron density of the aromatic ring leading to greater adsorption. The maximum inhibition efficiency of PCT and PPCT (98 - 99%) may be due to the interaction of π-electrons of phenyl, pyrazole rings, NH, NH_2 as well as a presence of a sulphur atom. In acidic medium, -NH_2 group is readily protonated, which might adsorb on the metallic surface *via.,* the negatively charged acid anions. PPCT was slightly higher than that of PCT, which can probably be explained by the presence of one additional phenyl ring in the molecule.

PAPM shows maximum efficiency of 97.62% and PHPM has 91.31%. The efficiency of the compound PAPM is due to the presence of electron releasing –NH_2 group ($\sigma = 0.16$) which enhances the delocalized π-electrons on the active centres of the molecule, where σ is the substituent constant (Hammett) and is a relative measure of the electron density at the reaction center[33]. *i.e.,* they act as additional anchoring sites for adsorption. PHPM has a –OH group in the ortho position, which is closer to the main adsorption centre. When compared to PAPM the lower I.E of PHPM may be attributed to the formation of intramolecular hydrogen bonding of the –OH hydrogen with the nitrogen atom of –NH group *via.,* the lone pair of electrons. The lone pair of electrons is therefore less readily available for protonation in acid medium. This hinders the electrostatic adsorption leading to lower inhibition when compared to PAPM. This phenomenon of ortho effect has been discussed by **Popova**[34] ***et al.,*** in their work in attempting to explain adsorption of molecules with ortho, meta and para substituents by Hammet equation[33]. PNPM has the lowest inhibition efficiency, because the m-NO_2 group ($\sigma = +0.71$) with the highest electrophilic character imparts the lowest inhibition efficiency. Possible hydrogentation of the NO_2 group in acid medium on the Fe surface also causes a decrease in efficiency of PNPM as the released heat of hydrogenation would aid the desorption of the molecule from the metal surface[35].

4.4 CONCLUSIONS

- All the investigated pyrazolines are effective inhibitors for the corrosion of mild steel in 1M H_2SO_4.
- The high inhibitive effect of pyrazolines was attributed to the adsorption of the inhibitor molecules on the metal surface and a protective film formation.
- Adsorption of the pyrazolines on mild steel in 1M H_2SO_4 solution at 303 K was a combination of both physisorption and chemisorption.
- Adsorption of the investigated pyrazolines obeyed Langmuir isotherm model.
- The ΔG°_{ads} and K_{ads} values justified that all the studied pyrazolines were strongly adsorbed on the mild steel surface.
- Electrochemical studies indicated that all the synthesized pyrazolines behave mainly as mixed inhibitors but predominantly cathodic type.
- SEM, AFM and FTIR studies confirmed the formation of a protective film of the inhibitor on the mild steel surface.

4.5 REFERENCES

1. K. Ajay Kumar, P. Jayaroopa, Int. J. Pharm. Tech., **5** (2013) 1473.
2. P.C. Sharma, S.V. Sharma, S. Jain, D. Singh, B. Suresh, Acta. Pol. Pharm., **66** (2009) 101.
3. S. Samshuddin, B. Narayana, B.K. Sarojini, R. Srinivasan, Vinayachandra, K.R. Chandrashekar, Der. Pharma. Chemica., **4** (2012) 587.
4. S.A. Ali, A.M. El-Shareef, R.F. Al-Ghandi, M.T. Saeed, Corros. Sci., **47** (2005) 2659.
5. Y. Abboud, A. Abourriche, T. Saffaj, Desalination, **237** (2009) 175.
6. R.L. Every, O.L. Riggs, Mat. Prot., **3** (1964) 46.
7. A. Popova, Corros. Sci., **49** (2007) 2144.
8. A.Y. El-Etre, J. Colloid. interf. Sci., (2007) 578.
9. Q. Qu, S. Jiang, W. Bai, L. Li, Electrochim. Acta., **52** (2007) 6811.
10. L. Herrag, B. Hammouti, S. Elkadiri, A. Aoumt, C. Jama, H. Vezin, F. Bentiss, Corros. Sci., **52** (2010) 3042.
11. A.K. Singh, S.K. Shukla, M.A. Quraishi, E.E. Ebenso, J. Taiwan Inst. Chem. Eng., **43** (2012) 463-472.
12. M. Abdallah, E.A. Heal, A.S. Fouda, Corros.Sci., **48** (2006) 1639.
13. Q.B. Zhang, Y.X. Hua, Electrochimica. Acta., **54** (2009) 1881.
14. K. Bayol, M. Kayakirilmaz, Erbil, Mater. Chem. Phys., **104** (2007) 74.
15. R. Touir, R.A. Belakhmima, M.E. Touhami, L. Lakhrissi, M. El Fayed, B. Lakhrissi, E. M. Essassi, J. Mater. Environ. Sci., **4** (2013) 921.
16. T.P. Zhao, G.N. Mu, Corros. Sci., **41** (1999) 1937.
17. L.B. Tang, G.N. Mu, G.H. Liu, Corros. Sci., **45** (2003) 2251.
18. L. Wang, Corros.Sci., **43** (2001) 1637.
19. D.A. Jones, Principles and prevention of corrosion, second edn. Prentice hall, Upper saddle river, NJ. (1996) 518.
20. F. Mansfeld, Electrochim. Acta., **35** (1990) 1533.
21. S.S. Mahmoud, M.M. Ahmed, R.A. El-Kasaby, Adv. Mater. Corros., **1** (2013) 6.
22. D. Jeyaperumal, Mater. Chem. Phys., **119** (2010) 478.
23. E.S. Ferreira, C. Glacomelli, F.C. Glacomelli, A. Spinelli, Mater. Chem. Phy., **83**, (2004) 129.
24. A. Petchiammal, S. Selvaraj, Pac. J. Sci. Tech., **14** (2013) 31.

25. A.S. Fouda, S. Rashwan, Y.K. Elghazy, Int. J. Adv. Res., **1** (2013) 568.
26. P. Dillmann, R. Balasubramaniam, G. Beranger, Corros. Sci., **44** (2002) 2231.
27. M.A. Chidiebere, E.E. Oguzie, L. Liu, Y. Li, F. Wang, Ind. Eng. Chem. Res., **53** (2014) 7670.
28. P. Mourya, S. Banerjee, R. Bala Rastogi, M. Mohan Singh, Ind. Eng. Chem. Res., **52** (2013) 12733.
29. I. Ahamad, R. Prasad, M.A. Quraishi, Corros. Sci., **52** (2010) 3033.
30. A. Kumar Singh, M.A. Quraishi, Corros. Sci., **52** (2010) 1529.
31. N.Hackerman, E.S. Snavely, J.S. Payne, J. Electrochem. Soc., **113** (1966) 677.
32. T. Murakawa, S. Nagaura, N. Hackerman, Corros. Sci., **7** (1967) 79.
33. L.P. Hammett, Physical organic chemistry, McGraw-Hill Book Co., New York.
34. A. Popova, M. Christova, S. Raicheva, E. Sokolova, Corros. Sci., **46** (2004) 1333.
35. A.S. Fouda, M.N. Moussa, Fl Taha, Al Elneanaa, Corros. Sci., **26** (1986) 719.